Electronic Supplementary Material (ESI) for Journal of Materials Chemistry C.
This journal is © The Royal Society of Chemistry 2017

Narrowband Spectrally Selective Near-infrared Photodetector Based on Up-conversion Nanoparticles/2D Hybrid

Nan Zhou,[a] *Bing Xu,*[a] *Lin Gan,* *[a] *Junpei Zhang,*[b] *Junbo Han,*[b] *and Tianyou Zhai**[a]

Keywords: MoS_2, UCNPs, narrowband, wavelength selectivity, near-infrared photodetector

a. *State Key Laboratory of Material Processing and Die and Mould Technology School of Materials Science and Engineering, Huazhong University of Science and Technology (HUST), Wuhan 430074, P. R. China.*
E-mail: zhaity@hust.edu.cn, ganlinust@hust.edu.cn

b. *Wuhan National High Magnetic Field Center, Huazhong University of Science and Technology (HUST). Wuhan, Hubei 430074, P. R. China*

Experimental Section

Synthesis of $NaYF_4$:Yb/Er@$NaYF_4$:Nd/Yb: The $NaYF_4$:Yb/Er@$NaYF_4$:Nd/Yb core-shell structured nanoparticles were synthesized by the co-precipitation method according to the published literature,[1] and the obtained $NaYF_4$:Yb/Er@$NaYF_4$:Nd/Yb up-converting nanoparticles, with an average diameter of 52 ± 1 nm, were re-dispersed in cyclohexane with designated concentration. The absorption spectrum of the UCNPs nanoparticles was measured by UV/Vis Spectrophotometer (LAMBDA 950, PerkinElmer), and the PL of the UCNPs nanoparticles and the hybrid were characterized by an EM-CCD camera (DU970P, Andor) equipped with a monochromator (SR500, Andor).

Synthesis of MoS_2 flakes: Schematic diagram for synthesis of MoS_2 using the CVD method is shown in Fig. S2, in which sapphire substrate was used to grow MoS_2 triangular flakes, and then treated with ultrasound in ethanol, acetone, and isopropyl alcohol for 15 min separately to remove organic surface. The growth process was carried out in a CVD system consisting of three temperature zones, of which zone II and zone I are for the precursors of $MoCl_5$ (99.999%, Alfa) and S (99.9%, Alfa) powders separately, and zone III is for the sapphire substrates. The growth conditions are as follows: the temperature of S powder was controlled to be slightly above the melting point of sulfur (120 ℃) and the temperature of substrate was set as 800 ℃, the growth duration was about 10 min, the heating rate was about 25 ℃/min, and the carrier gas was about 50 sccm N_2 etc. The MoS_2 flakes were characterized by an optical microscope (BX51, OLMPUS), a transmission electron microscope (Tecnai G2 F30, FEI) equipped with an energy-dispersive X-ray (EDX), a confocal Raman/PL system (HR-800, HORIBA Jobin Yvon), an atomic force microscope (SPM9700, Shimadzu), and X-ray fluorescence diffraction (7000S, Shimadzu, radiation).

Device Fabrication and Characterization: Monolayer MoS_2 flakes are deposited on sapphire substrates and then transferred on top of SiO_2（300 nm)/Si substrate firstly. Electrodes are fabricated by electron beam lithography (Nexdep, Angstrom Engineering), followed by thermal evaporation of Ti (10 nm) and Au (50 nm), respectively. $NaYF_4$:Yb/Er@$NaYF_4$:Nd/Yb nanoparticles film coated with oleate-ligand were then spin-coated over the MoS_2 device, about 50 nm thick. The film was pretreated with hydrazine[2] to remove the oleic acid shell of $NaYF_4$:Yb/Er@$NaYF_4$:Nd/Yb nanoparticles, which would create a large barrier for carrier transport. Then the devices were annealed at 300 ℃ inside a vacuum furnace to enhance the contact of two materials and remove the surface of oleic acid thoroughly. For photodetection under 808 nm or 980 nm laser, the photocurrent were collected by a semiconductor characterization system (4200SCS, Keithley) at room temperature, and time-resolved photocurrent were collected a current meter.

Characterization

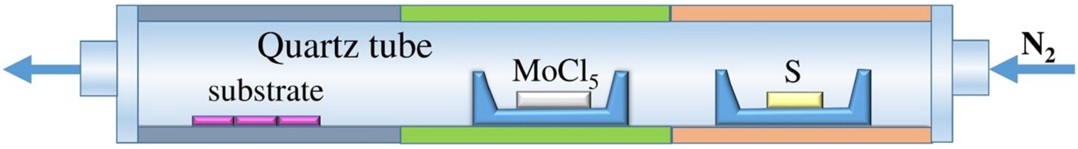

Fig. S1 Schematic diagram for synthesis of layered MoS_2 using the chemical vapor deposition (CVD) method.

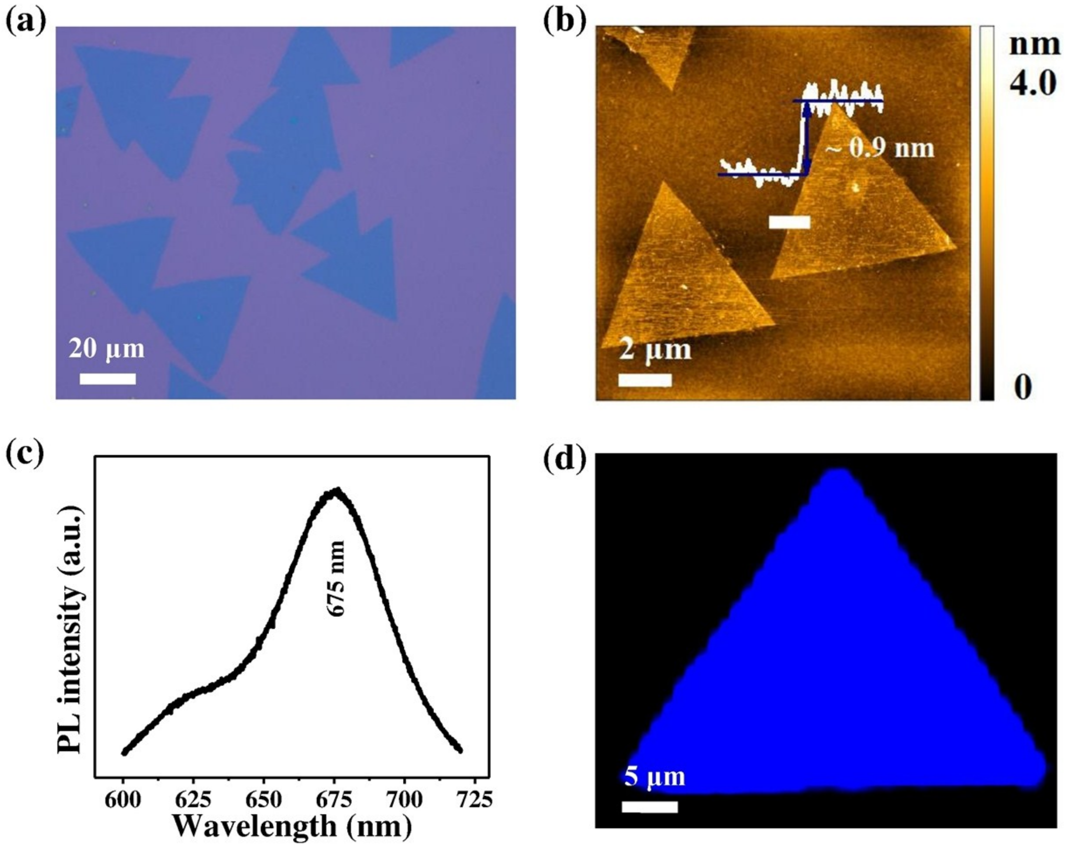

Fig. S2 (a) Optical image of CVD-synthesized MoS_2 flakes. (b) A typical AFM image of the MoS_2 flakes on SiO_2 substrate and the height profile implying a thickness of ~ 0.9 nm. (c) and (d) PL spectrum and the PL intensity mapping of MoS_2 flake on SiO_2 substrate.

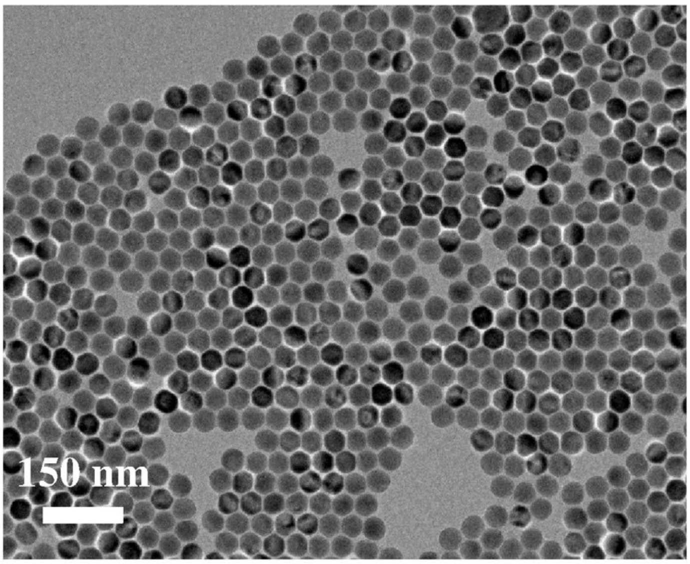

Fig. S3 Low-magnification TEM image of core-shell structured UCNPs ($NaYF_4$:Yb/Er@$NaYF_4$:Nd/Yb).

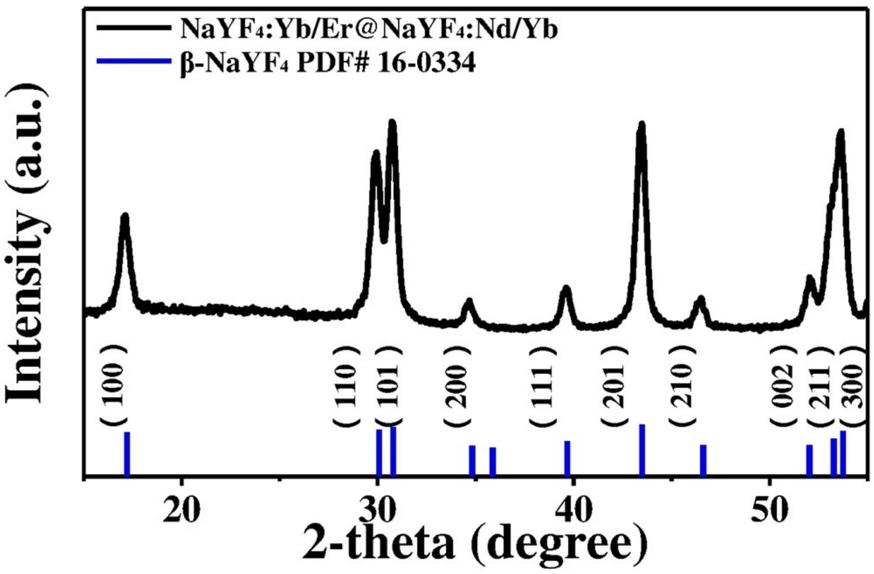

Fig. S4 XRD pattern of $NaYF_4$:Yb/Er@$NaYF_4$:Nd/Yb nanoparticles.

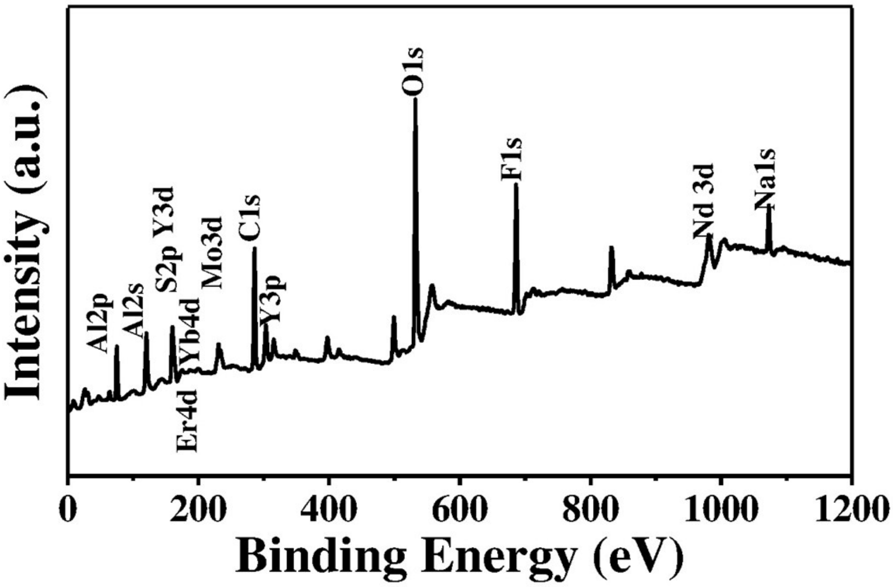

Fig. S5 XPS spectrum of (NaYF_4:Yb/Er@NaYF_4:Nd/Yb)/MoS_2 hybrid on sapphire substrate.

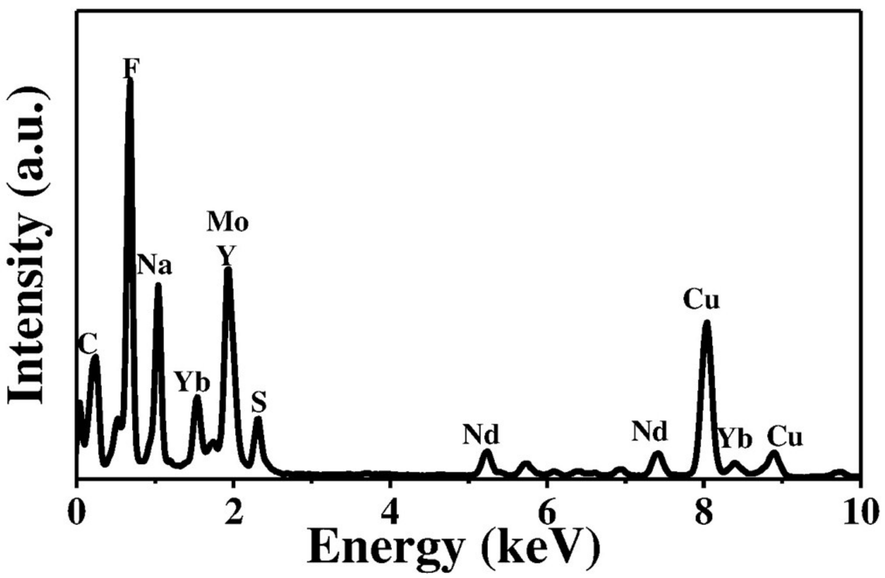

Fig. S6 TEM-based energy-dispersive X-ray (TEM-EDX) of ($NaYF_4$:Yb/Er@$NaYF_4$:Nd/Yb)/MoS_2 hybrid, indicating the presence of elements of Na, Y, F, Yb, Nd, Mo and S.

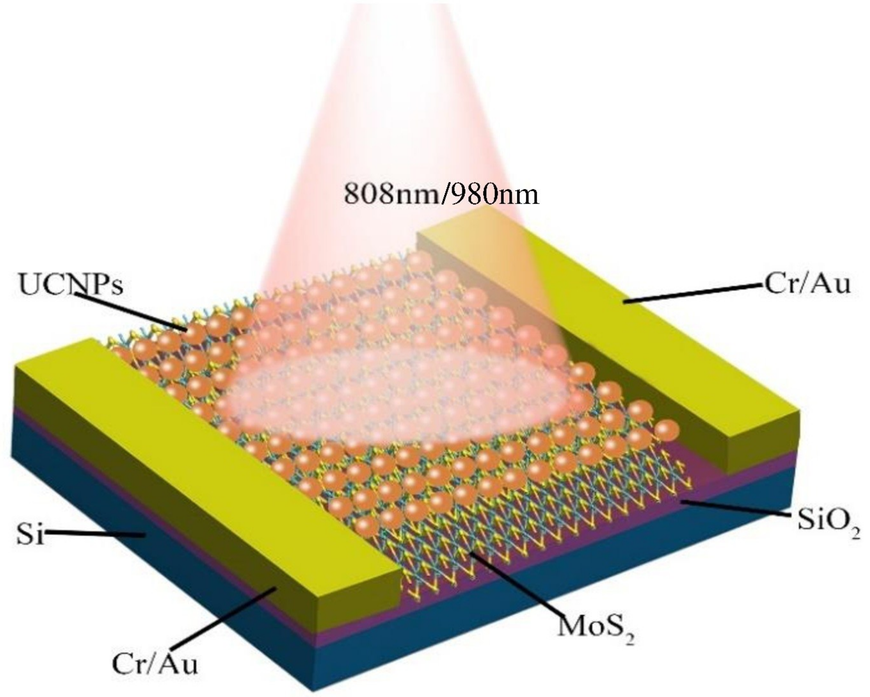

Fig. S7 3D view of the ($NaYF_4$:Yb/Er@$NaNdF_4$:Nd/Yb)/MoS_2 hybrid device.

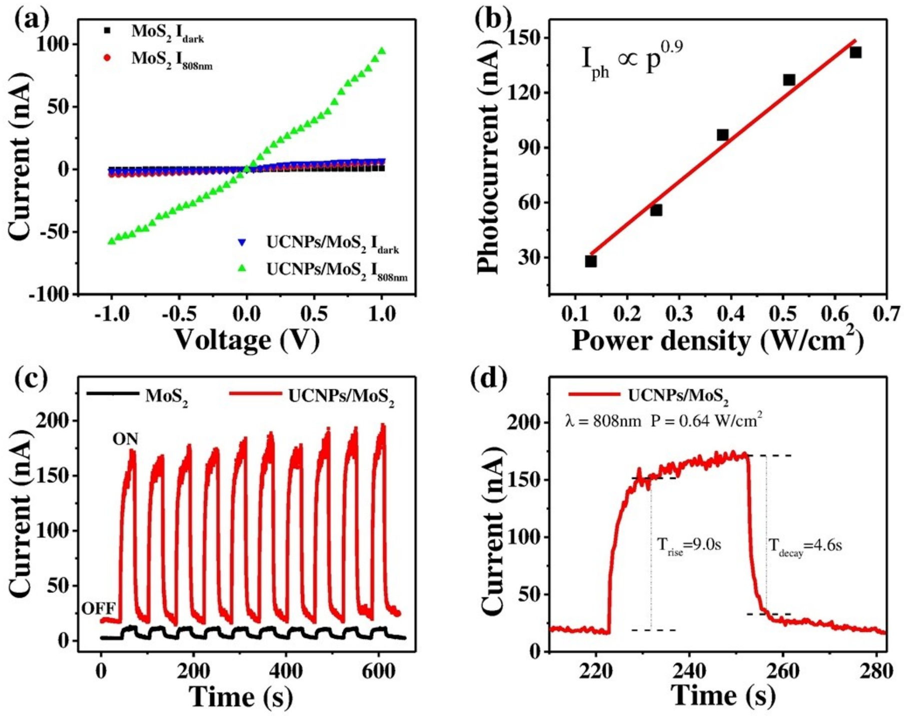

Fig. S8 Optoelectronic properties of the ($NaYF_4$:Yb/Er@$NaYF_4$:Nd/Yb)/MoS_2 hybrid and single-layer MoS_2 photodetectors under 808 nm illumination. (a) The current-voltage (I-V) characteristics of the same devices, under dark and 808 nm laser. (b) Photocurrent of the hybrid device dependent on illumination intensity. (c) The stable and repetitive switching characteristic curves of the both devices under dark and the same laser power, with a bias of 1V. (d) Time-resolved photocurrent rise and decay rate after 808 nm laser switching ON and OFF in ambient conditions.

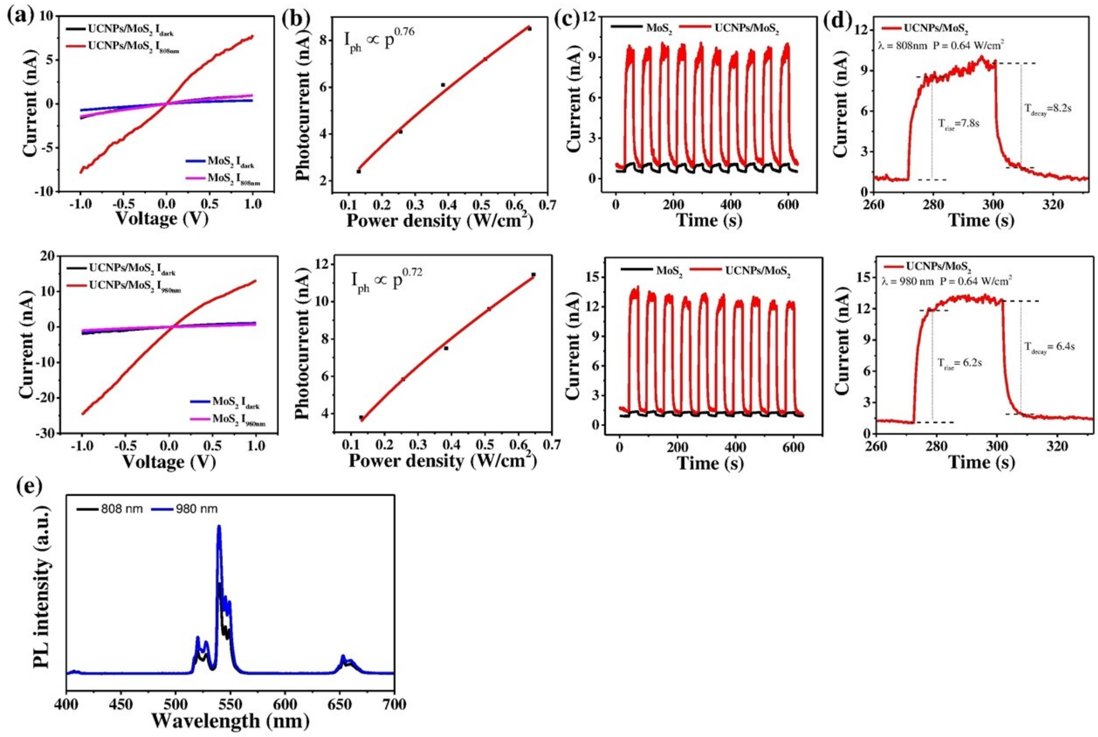

Figure S9. Optoelectronic properties based on the same MoS_2 device before and after UCNPs compositing under 808 nm (upper) and 980 nm (lower) illumination, respectively. (a) The current-voltage (I-V) characteristics of the same devices, under dark and illumination. (b) Photocurrent of the hybrid device dependent on illumination intensity. (c) The stable and repetitive switching characteristic curves of the both devices under dark and illumination, with a bias of 1V. (d) Time-resolved photocurrent rise and decay rate switching ON and OFF in ambient conditions. (e) PL spectra of UCNPs dispersed in cyclohexane （0.2 mol/L）under 808 nm (black) and 980 nm (blue) laser illumination.

Comparing with the photoresponse data under 808 nm and 980 nm illumination, interestingly, we can find the hybrid device show a higher photoresponsivity and faster response rate under 980 nm than under 808 nm laser. The higher photoresponsivity can be attributed to the higher up-converting efficiency of UCNPs under 980 nm light as shown in fig S9e, which further result in higher photocurrent then photoresponsivity in the hybrid device. The faster response rate under 980 nm can also be understood in similar way. As we know, the response rate is strongly negative related to the life time of carriers, i.e. longer carrier lifetime, slower response rate and vice versa. The photocurrent under 980 nm is obviously larger than that under 808 nm, evidencing the carrier density under 980 nm is larger than that under 808 nm as well. Therefore, we speculate that the faster response under 980 nm is attributed to the shorted lifetime of carriers under 980 nm due to high density of carrier induced increased recombination rate, which also supported by the fitting exponent α shown in Fig. S9b. The exponent α under 980 nm is 0.72 that is slightly smaller than 0.76 under 808 nm, suggesting a higher recombination rate under 980 nm.[3, 4] It is worth to note that these analysis only valid for the comparison of data on the same device, the case would be altered for comparison between different devices because the fitting component α is complex and related to various factors.[5]

Notes and references

1 B. Xu, X. Zhang, W. Huang, Y. Yang, Y. Ma, Z. Gu, T. Zhai, Y. Zhao, J. Mater. Chem. B, 2016, 4, 2776-2784.

2 C. Yan, A. Dadvand, F. Rosei, D. F. Perepichka, J. Am. Chem. Soc., 2010, 132, 886-8869.

3 W. Zhang, J. K. Huang, C. H. Chen, Y. H. Chang, Y. J. Cheng and L. J. Li, Adv. Mater., 2013, 25, 3456-3461.

4 F. Gonzalez-Posada, R. Songmuang, M. Den Hertog and E. Monroy, *Nano Lett.*, 2012, **12**, 172-176.

5 H. Kind, H. Yan, B. Messer, M. Law, P. Yang, *Adv. Mater.,* 2002, **14,** 158-160.